SPECIAL ISSUE RESEARCH ARTICLE

WILEY

Fat crystals: A tool to inhibit molecular transport in W/O/W double emulsions

Veronique Nelis[1,2] 🆔 | Arnout Declerck[1] | Lien Vermeir[1] 🆔 | Mathieu Balcaen[1] | Koen Dewettinck[2] | Paul Van der Meeren[1]

[1] Particle and Interfacial Technology Group, Faculty of Bioscience Engineering, Ghent University, Ghent, Belgium

[2] Laboratory of Food Technology and Engineering, Faculty of Bioscience Engineering, Ghent University, Ghent, Belgium

Correspondence
Veronique Nelis, Particle and Interfacial Technology Group, Faculty of Bioscience Engineering, Ghent University, Coupure Links 653, B-9000 Ghent, Belgium.
Email: veronique.nelis@ugent.be

Funding information
Hercules Foundation, Grant/Award Number: AUGE-09-029; Fund for Scientific Research—Flanders (FWO-Vlaanderen)

Abstract

Water-in-oil-in-water (W/O/W) double emulsions are a promising technology for encapsulation applications of water soluble compounds with respect to functional food systems. Yet molecular transport through the oil phase is a well-known problem for liquid oil-based double emulsions. The influence of network crystallization in the oil phase of W/O/W globules was evaluated by NMR and laser light scattering experiments on both a liquid oil-based double emulsion and a solid fat-based double emulsion. Water transport was assessed by low-resolution NMR diffusometry and by an osmotically induced swelling or shrinking experiment, whereas manganese ion permeation was followed by means of T_2-relaxometry. The solid fat-based W/O/W globules contained a crystal network with about 80% solid fat. This W/O/W emulsion showed a reduced molecular water exchange and a slower manganese ion influx in the considered time frame, whereas its globule size remained stable under the applied osmotic gradients. The reduced permeability of the oil phase is assumed to be caused by the increased tortuosity of the diffusive path imposed by the crystal network. This solid network also provided mechanical strength to the W/O/W globules to counteract the applied osmotic forces.

KEYWORDS
fat crystals, LR-^{1}H-NMR diffusometry, molecular transport, osmotic pressure, T_2-relaxometry, W/O/W double emulsion

1 | INTRODUCTION

Water-in-oil-in-water (W/O/W) double emulsions are composed of oil globules dispersed in a continuous aqueous phase and of which the oil globules carry dispersed water droplets. Thanks to this typical structure, W/O/W double emulsions are a promising technology for encapsulation applications of water soluble active agents. As a further consequence, W/O/W emulsions gain increasing interest in the pharmaceutical and food industry.[1,2] Long-term retention of the entrapped compounds in the internal water droplets is hereby a key parameter. Unfortunately, next to the common destabilization processes encountered for classical single emulsions (e.g., Ostwald ripening, creaming, coalescence, and flocculation[3]), W/O/W-type emulsions are prone to molecular transport

---

Abbreviations: EV, enclosed water volume; HOSO, high oleic sunflower oil; PFG-NMR, pulsed field gradient NMR; PGPR, polyglycerol polyricinoleate; PGSTE, pulsed gradient stimulated echo pulse sequence; SFC, solid fat content; sPMF, soft palm mid fraction; STE, stimulated echo pulse; W/O, water-in-oil; W/O/W, water-in-oil-in-water; WC, water content; Δ, diffusion delay time

of both water and encapsulated compounds through the oil phase.[4] This phenomenon is commonly encountered in W/O/W emulsions formulated with liquid oil.[5]

Over the years, a lot of research has been conducted on W/O/W emulsion stability with special attention to diffusion-driven molecular transport and to the unveiling of the underlying mechanisms governing this type of destabilization.[6–14] Next to diffusion of single molecules, diffusion-mediated transport has been described in literature.[4,8] Four assisted transport mechanisms have been defined in case of water transport, that is, transport through spontaneous emulsification, reversed micelles, thinned lamellae, and hydrated surfactants.[1,4,8,12,15–19] Most of the studies regarding quantification of the (water) transport kinetics illustrate the importance of the W/O/W formulation and focus mainly on osmotic regulation, emulsifier characteristics and concentrations, or on the physical state of matter of the internal water droplets (e.g., gelation of the internal water[20,21]). Apart from the viscosity of the oil phase,[4,11,22] the impact of the nature of the oil phase is largely unexplored considering exchange kinetics.

Taking into account that oil molecules significantly experience restricted diffusion due to a fat crystal network with a minimal solid fat content (SFC) of 50%,[23] it seems reasonable to assume that water and solute molecules will experience comparable SFC-dependent restrictions on diffusion when travelling through the fat phase. In case of bulk crystallization in the oil phase of an osmotically balanced W/O/W double emulsion, an increasing SFC has been noted to reduce the release rate of encapsulated marker compounds[24–26] and to reduce the water exchange kinetics between the water compartments.[27,28] Herzi and Essafi[26] recently demonstrated that the release of magnesium ions was dependent on the SFC provided that the oil phase of the W/O/W globule consisted of a continuous crystal network. In case of an osmotically imbalanced core-shell type W/O/W system, Guery et al.[25] did not state any increase in globule dimensions nor loss of the globule structure upon large deformation stresses due to a positive osmotic gradient. They argued that even a limited water flux through the solid shell built up an internal pressure which facilitated leakage of enclosed chloride ions to the continuous aqueous phase. Moreover, leakage increased with an enlarging positive osmotic gradient. Hence, the applied stress facilitated chloride permeation through the robust fat crystal shell. Other researchers concluded that fat crystals located at the internal W/O interface could not only stabilize the internal water droplets by a Pickering mechanism but could also successfully withstand or reduce the release of salts.[29–33] These latter W/O/W systems are typically characterized by a thin solid shell at the W/O

interface. Apart from the work of Herzi and Essafi,[26] little attention has been paid to the physicochemical properties of the solid fat in network crystallized W/O/W double emulsions. In the field of solid lipid particles for hydrophobic drug delivery, it is already well established that release profiles (e.g., burst or sustained release) are governed by the physicochemical and structural properties of the fat matrix.[3,34–37]

This contribution focuses on the effect of the physical state of the oil phase on the molecular exchange kinetics in W/O/W-type emulsions. Molecular transport through the oil phase of either a liquid oil-based double emulsion or a solid fat-based double emulsion was assessed by three different types of experiments in order to evaluate the functionality of the solid fat to act as a physical barrier against molecular transport. First, we assessed the resistance of the fat wall to water exchange by means of Δ-dependent NMR diffusometry under isotonic conditions. Moreover, osmotically induced swelling or shrinking experiments were used to shed more light on the ability of the fat crystals to withstand an external osmotic force. Herewith, water transport was evaluated by monitoring the globule size as a function of time under nonisotonic conditions. Third, the permeation of manganese cations through the oil phase was followed by means of T_2-relaxometry during a long term storage experiment.

2 | MATERIALS AND METHODS

2.1 | Materials

In this study, we examined a W/O/W emulsion formulated with two types of fat: soft palm mid fraction (sPMF) and high oleic sunflower oil (HOSO), a crystallizing and noncrystallizing fat, respectively, at the experimental temperature of 5°C. sPMF (pmf28: SFC of 0.8% at 35°C, 46% at 20°C, and 75% at 10°C; iodine value = 42; 51.3% C16:0 and 36.4% C18:1-cis) was a kind gift of Vandemoortele (Izegem, Belgium), whereas HOSO (iodine value = 87; 83.8% C18:1) was acquired from Contined B.V. (Bennekom, The Netherlands). The lipophilic emulsifier polyglycerol polyricinoleate (PGPR 4175; minimum 75% n-glycerols with n = 2, 3, and 4; maximum 10% m-glycerols with $m \geq 7$), the hydrophilic emulsifier sodium caseinate (5.5% moisture, 96% protein on dry matter), and the stabilizer xanthan gum (food grade, FF) were kindly provided by Palsgaard A/S (Juelsminde, Denmark), Armor Protéines (Saint Brice en Cogles, France), and Jungbunzlauer (Vienna, Austria), respectively. KCl and the antimicrobial agent NaN₃ were purchased from VWR Chemicals (BDH Prolabo, Leuven, Belgium) and Acros Organics (Geel, Belgium),

respectively. All above-mentioned chemicals were of analytical grade.

2.2 | W/O/W double emulsion production

30/20/50 (w/w/w) W/O/W double emulsions were prepared in a two-step emulsification procedure. In the first step, a 60/40 (w/w)% water-in-oil (W/O) emulsion was produced by slowly adding (over about 1.5 min) an aqueous solution (0.1 M KCl, 0.02 wt% NaN_3) to an oil phase (5.0 wt% PGPR 4175 in sPMF or HOSO) while mixing for 7.5 min in total with an Ultra-Turrax (IKA Werke) T50 basic rotor G45F at a mixing speed of 5,200 rpm. Both the oil and aqueous phase were heated to 60°C prior to emulsification. In the second step, this primary W/O emulsion was added to a second aqueous phase in a 50/50 (w/w) ratio. This second aqueous phase consisted of 0.1 M KCl, 0.02 wt% NaN_3, 1.25 wt% sodium caseinate, and 0.3 wt% xanthan gum and was stirred overnight at room temperature to allow hydration and dissolution of the sodium caseinate and xanthan gum. Both the primary emulsion and the second aqueous phase were heated to 60°C prior to emulsification. The sample was mixed for 1 min with an Ultra-Turrax IKA Werke T25 basic rotor S25KV-25G-IL at 6,500 rpm. The produced pre-emulsion was further homogenized by passing it once through a Microfluidizer M110S, which amplifies the driving air pressure of 1.25 bar with a factor of 140. The heating coil of the Microfluidizer was set at 60°C by use of a water bath. After production, the obtained W/O/W emulsions were immediately placed in a refrigerator set at 5°C and were subsequently stored overnight prior to the evaluation of molecular transport by the osmotic experiment, NMR diffusometry, and T_2-relaxometry. Any small pressure difference will be immediately adjusted after production, hence, generating an osmotically stable double emulsion. In case of the osmotic experiment at 40°C, a part of the stored W/O/W_{sPMF} emulsion was heated to 40°C before carrying out the experiment.

2.3 | W/O/W characterization and evaluation of molecular flux

2.3.1 | Static laser light scattering

Determination of the globule size distribution
To characterize the W/O/W double emulsions, the fat globule size distribution was determined based on Mie scattering by laser diffraction using a Mastersizer 3000 (Malvern Ltd, UK) with the refractive indices of the dispersed and continuous phase set at 1.53 + 1.0i and 1.33, respectively. The emulsions were added dropwise to the

dispersing unit Malvern Hydro MV, set at a stirring speed of 2,000 rpm, until an obscuration between 10% and 20% was reached. The dispersing unit contained an isotonic solution (0.1 M KCl). The droplet diameter is given as the volume-weighted average diameter ($D_{4,3}$).

Osmotically induced swelling or shrinking experiment
The impact of the osmotically induced water flux on the structure evolution of the W/O/W globules was evaluated performing 50 consecutive measurements, which were taken with a time interval of 23 s. The emulsion was added when the solution in the dispersing unit had the desired temperature (5°C or 40°C). The temperature was regulated by connecting the Mastersizer 3000 to a water bath. All other settings were identical to the settings used to determine the globule size distribution for characterization of the W/O/W double emulsions. An osmotic pressure difference along the fat layer of the double emulsion was governed by diluting the initially isotonic W/O/W sample in the dispersion unit of the device, which was filled with a hypotonic (distilled water), isotonic (0.1 M KCl), or hypertonic (0.5 M KCl) solution. As such, KCl is the main regulator of both the internal and external osmotic pressure. For the calculation of the osmotic pressure, we neglected all other solute contributions because they are only present in minor amounts. According to the van't Hoff law, the osmotic gradient (defined as the difference in osmotic pressure between the internal and external aqueous phase) was 462 and 520 kPa in the hypotonic experiment at 5°C and 40°C, respectively, whereas it was −1,849 and −2,082 kPa in the hypertonic experiment at 5°C and 40°C, respectively. At least two independent experiments were conducted with W/O/W emulsions that were stored for 1 day in a refrigerator set at 5°C. In case of the osmotic experiment at 40°C, a part of the stored W/O/W_{sPMF} emulsion was heated to 40°C before carrying out the experiment.

2.3.2 | Low-resolution NMR

All NMR experiments were conducted on a Maran Ultra 23-MHz NMR analyzer (Oxford Instruments, UK), thermostatically regulated at 5°C, using the Oxford Instruments' acquisition software RINMR. About 3 g of emulsion was transferred to a 1.8-cm diameter NMR tube. Samples were measured after 1 day of storage at 5°C. A spacer of 3.0 cm was used to place the sample within the detection window.[38]

Pulsed field gradient NMR diffusometry
Pulsed field gradient (PFG) NMR diffusometry experiments were conducted using a stimulated echo pulse

sequence, preceded by an inversion recovery experiment to suppress the fat signal. A fixed gradient pulse duration (δ) of 2.5 ms and a diffusion delay time (Δ) of 60 and 220 ms were used, whereas the gradient strength (G) ranged from 0 to 2.09 T/m (16 increments). The optimal repression constant (τ_0) of both the sPMF and HOSO oil phase were determined using bulk oil samples and were 47.45 and 53.75 ms, respectively. The normalized signal (I/I_0) is described by the Stejskal and Tanner[39] equation (Equation 1). Herewith, γ is the gyromagnetic ratio of the protons (2.675×10^8 s^{-1} T^{-1}), D is the water diffusion coefficient, and I_0 is the signal intensity without gradient pulse. For a schematic outline of the pulsed gradient stimulated echo pulse sequence, we refer to Vermeir et al.[27] In such a typical diffusion experiment, the translational molecular water displacement is probed during a characteristic observation time, that is, the Δ-value.

This experimental design enables to distinguish the two water compartments (i.e., internal and external water) of a double emulsion. The enclosed water volume (EV) is defined as the fraction of the total water that is present as internal water. Given a constant Δ and δ and a varying G, a simple biexponential fit (Equation 2) to the experimental echo attenuation generates a good approximation of the EV,[27] assuming a monodisperse water droplet size distribution. In the event of water transport between the internal and external water phase (i.e., extradroplet water exchange) in W/O/W double emulsions, the attenuated diffusion curve depends on the applied Δ-value, which renders apparent EV values. Vermeir et al.[27] showed a linear relationship between the apparent EV of a W/O/W emulsion and the Δ-value. The real EV can thus be approximated by linear extrapolation of the apparent EV's as previously described[27] and is referred to as $EV_{\Delta \to 0}$. The biexponential fit and the linear extrapolation were conducted using Sigmaplot 14 software.

$$I(G, \delta, \Delta) = I_0 . \exp\left[-q^2 . D . \left(\Delta - \frac{\delta}{3}\right)\right], \quad (1)$$

with $q^2 = (\delta . \gamma . G)^2$

$$\begin{aligned} E(G^2) &= \frac{I}{I_0} \\ &= EV . \exp[-a . G^2] \\ &+ (1 - EV) . \exp[-b . G^2] \text{ (for a constant } \delta \text{ and } \Delta). \end{aligned} \quad (2)$$

SFC and WC

SFC and water content (WC) of the W/O/W double emulsions were determined by means of a deconvolution method as previously described[40] using a free induction decay (FID) CPMG sequence, whereby the Carr Purcell

Meiboom Gill (CPMG) experiment was sequenced after the FID experiment in one combined measurement. The applied FID-CPMG sequence was carried out using a 90° radio frequency pulse of 7.9 μs followed by successive 180° pulses of 15.8 μs to restore the uniformity of the magnetic field. The time between the successive 180° pulses was 300 μs. The dead time per scan was 7.5 μs, and the dwell time was 0.1 μs. The FID data were collected from 15.4 to 50 μs, whereas the CPMG data were acquired from 304 μs to 1.23 s. The obtained FID-CPMG data were fitted with a summation of one Gaussian function and a set of exponential functions (Equation 3). This model fit was based on the work of Trezza et al.[41] but simplified and adjusted for our situation. As such, the solid contribution in the FID data was fitted to a Gaussian function, whereas the liquid signal in the CPMG data was fitted to a summation of exponential functions using CONTIN-analysis.[42] The liquid oil signal was assigned to $T_{2,i}$ values below 200 ms, whereas the water signal was assigned to $T_{2,i}$ values above 200 ms. The discrimination between the solid fat, liquid oil, and water fraction in the W/O/W samples, by this FID-CPMG deconvolution method, enabled to determine the SFC (Equation 6) and WC (Equation 7). The values for the SFC and WC are both proton-weighted percentages. All fitting procedures were performed using MATLAB R2016a software. For CONTIN-based analyses, the freely available Matlab script (rilt.m) was used.

$$I_{FID-CPMG, fit}(t) = I_{0, Solid\ fat} . e^{-0.5\left(\frac{t}{T^*_{2, Solid}}\right)^2} + \sum_{i=1}^{N_G}\left(I_{0,i} . e^{-\left(\frac{t}{T_{2,i}}\right)}\right). \quad (3)$$

Hereby, N_G is the number of grid points in the T_2-distribution, which was fixed at 50 and logarithmically spaced from 100 μs to 100 s. With $N_G = N_{G,\ Water} + N_{G,\ oil}$,

$$I_{0, Liquid\ oil} = \sum_{i=1}^{N_{G,Oil}} I_{0,i}, \quad (4)$$

$$I_{0, Water} = \sum_{i=N_{G,Oil}+1}^{N_G} I_{0,i}, \quad (5)$$

$$SFC_{fat\ phase} = \frac{I_{0, Solid\ fat}}{I_{0, Solid\ fat} + I_{0, Liquid\ oil}} * 100\%, \quad (6)$$

$$Water\ content = \frac{I_{0, Water}}{I_{0, Solid\ fat} + I_{0, Liquid\ oil} + I_{0, Water}} * 100\%. \quad (7)$$

T$_2$-relaxation

T$_2$-relaxation (i.e., transverse relaxation) measurements were conducted to evaluate the MnCl$_2$ permeation through the oil layer during long-term storage using the same CPMG sequence and experimental parameters as used for the FID-CPMG experiment. The obtained signal decay was converted in a continuous distribution of T$_2$-relaxation times by the software WinDXP 1.8.1.0 (Oxford Instruments, UK). Prior to analysis, data reduction was carried out by selecting 511 prune points (logarithmically spaced) out of 8,192 points; 2.5% (v/v) 10-mM MnCl$_2$ was added to the continuous phase of the W/O/W double emulsions after overnight storage at 5°C. This paramagnetic probe was added in sufficiently high amounts to obtain a good signal separation of the water compartments and low enough to limit a dilution effect and osmotic imbalances.[43] The evolution of the T$_2$-distribution was followed during a storage period of 35 days at 5°C. The first experiment was performed 20 min after addition of MnCl$_2$ and is further referred to as day 0.

2.3.3 | Microstructure visualization

Verification of the double emulsion structure was performed by observation using a light microscope (Olympus Nihon Kohden) equipped with a hundredfold oil immersion objective coupled to a digital camera (AxioCam ERc 5S). Prior to image acquisition, the double emulsions were diluted tenfold in the W$_2$ aqueous phase.

The microstructure of the solid fat-based double emulsion was visualized using cryogenic scanning electron microscopy (cryo-SEM). The double emulsion sample was placed on a stub and quickly frozen in slushed nitrogen (−210°C). The stub was then mounted on the sample holder in the preparation chamber (PP3010T Cryo-SEM Preparation System, Quorum Technologies) where the sample was fractured at −150°C, sublimated, sputter-coated with platinum, and visualized with a Jeol JSM-7100F scanning electron microscope

(Jeol [Europe] B.V., Zaventem, Belgium) using an accelerating voltage of 3 kV.

2.3.4 | Statistical analysis

Regarding the comparison of group means, statistical analysis was performed using SPSS Statistics 24 at a 5% significance level. An independent samples t-test or a paired samples t-test was carried out on group means of two independent or paired samples, respectively. Concerning model fitting of the NMR-diffusion data by a biexponential fit to estimate the EV, the R^2 value was calculated. Each sample was analyzed in triplicate unless stated otherwise.

3 | RESULTS AND DISCUSSION

3.1 | W/O/W double emulsion characterization

The W/O/W$_{sPMF}$ double emulsion was characterized by a SFC of 79.9 ± 0.3% (on fat basis) at 5°C, an experimentally determined WC of 81.1 ± 0.5% and a fat globule diameter (D$_{4,3}$) of 2.5 ± 0.0 μm. The D$_{4,3}$ of the W/O/W$_{HOSO}$ emulsions was 2.9 ± 0.0 μm. The W/O/W$_{sPMF}$ emulsion had a monodisperse globule size distribution profile, whereas the W/O/W$_{HOSO}$ emulsion had a quasimonodisperse distribution: a dominant peak around 2 μm with a very small peak around 20 μm. Estimation of the real EV by linear extrapolation to a Δ-value of 0 ms generated an EV$_{Δ→0}$ of 14.6 ± 0.1% and 20.8 ± 0.1% for the W/O/W$_{HOSO}$ and the W/O/W$_{sPMF}$ double emulsions, respectively, after overnight storage at 5°C. It thus seems that the W/O/W$_{sPMF}$ emulsion could significantly better retain the internal water than the W/O/W$_{HOSO}$ emulsion. The rather low yield of internal water is due to microfluidization. However, as such creaming was largely prevented.

Light microscopy imaging of the W/O/W$_{sPMF}$ and W/O/W$_{HOSO}$ double emulsions confirmed the W/O/W-type structure (Figure 1). A distinct fat globule shape is
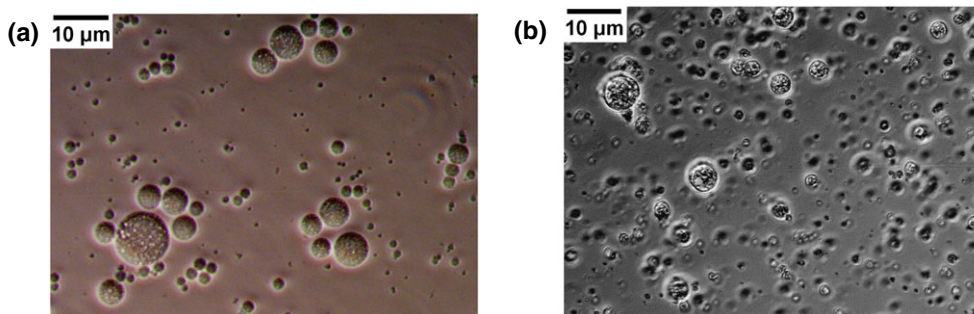

FIGURE 1 Light microscopy images of the double emulsions: (a) W/O/W$_{Hoso}$ and (b) W/O/W$_{sPMF}$, after overnight storage at 5°C. HOSO: high oleic sunflower oil; sPMF: soft palm mid fraction; W/O/W: water-in-oil-in-water

noted for the W/O/W$_{sPMF}$ globules: smooth, round globules are perceived for the W/O/W$_{HOSO}$ emulsion whereas a coarse, irregular round shape is observed for the W/O/W$_{sPMF}$ emulsion. The latter distorted round shape is ascribed to a fat crystal network, which dictates the shape of the W/O/W$_{sPMF}$ globules. sPMF consists mainly of nonsurface active triacylglycerols,[44] which suggests predominantly bulk crystallization in the oil volume of the W/O/W globules. Cryo-SEM images of the W/O/W$_{sPMF}$ (Figure 2a,b) validate the small fat globule size measured by light scattering and reveal the existence of a crystalline fat matrix. Furthermore, the observed cavities in the fat globules confirm that internal water droplets were present before sublimation of the sample. It can be deduced from the cryo-SEM images that the dimensions of the inner droplets of the W/O/W emulsions are in the submicron range. sPMF crystallization is expected to induce a continuous fat crystal network in the bulk volume of the oil phase of the W/O/W globule, which imposes tortuosity to the migration path of diffusing compounds in the oil phase,[45] whereas the presence of PGPR at the oil–water interface is thought to impede the formation of a crystal shell.[31]

3.2 | Impact of an osmotic gradient on W/O/W double emulsion stability

The sensitivity of a solid fat-based double emulsion (i.e., the W/O/W$_{sPMF}$ double emulsion at 5°C [W/O/W$_{sPMF,5°C}$]) towards an osmotic stress was compared with two liquid oil-based double emulsions, that is, the W/O/W$_{sPMF}$ double emulsion at 40°C (W/O/W$_{sPMF,40°C}$) and the W/O/W$_{HOSO}$ double emulsion at 5°C (W/O/W$_{HOSO,5°C}$), in order to relate the swelling or shrinking behavior to the physical state of the oil phase. Differential scanning calorimetry data (added in the Supporting Information) revealed that bulk sPMF and HOSO are fully melted, and thus liquid, at 40°C and 5°C, respectively.

In addition, the SFC (determined by NMR) of the W/O/W$_{sPMF}$ double emulsions was 0% at 35°C.[46] The experimental setup (section 2.3.1) allows to observe the swelling or shrinking behavior of the double emulsion globules due to an applied external osmotic pressure.

3.2.1 | Control conditions: Equal osmotic pressure

A control experiment under isotonic conditions was conducted to assess the stability of the W/O/W emulsions under constant stirring (2,000 rpm) in the dispersion unit during the experimental time frame. Given the straight contour lines in Figure 3a and 3c, the globule size distribution of the W/O/W$_{sPMF,5°C}$ and W/O/W$_{HOSO,5°C}$ double emulsions did not alter under the experimental conditions. Hence, at 5°C, the stirring did not affect the globule size distribution within the considered time frame. The $D_{4,3}$ obtained from the first and last distribution profile was 2.5 ± 0.0 μm and 2.4 ± 0.1 μm, respectively, for the W/O/W$_{sPMF,5°C}$ emulsion, whereas for the W/O/W$_{HOSO,5°C}$ emulsion, a $D_{4,3}$ of 2.9 ± 0.0 μm and 2.9 ± 0.3 μm was noted. At 40°C, the first and last distribution profiles of the W/O/W$_{sPMF,40°C}$ emulsion were not entirely identical (Figure 3b): No peak shift was observed but rather a limited peak broadening. This observation might reflect some globule coalescence occurring during the measurement.

3.2.2 | Effect of a positive osmotic gradient

Osmotically induced swelling of the W/O/W globules due to a positive osmotic gradient was hypothesized to only take place provided that a permeable, liquid oil phase was present. This condition was met for the W/O/W$_{HOSO,5°C}$ and W/O/W$_{sPMF,40°C}$ emulsions. The globule size distribution profile of the W/O/W$_{HOSO,5°C}$ double emulsion upon dilution in a hypotonic solution
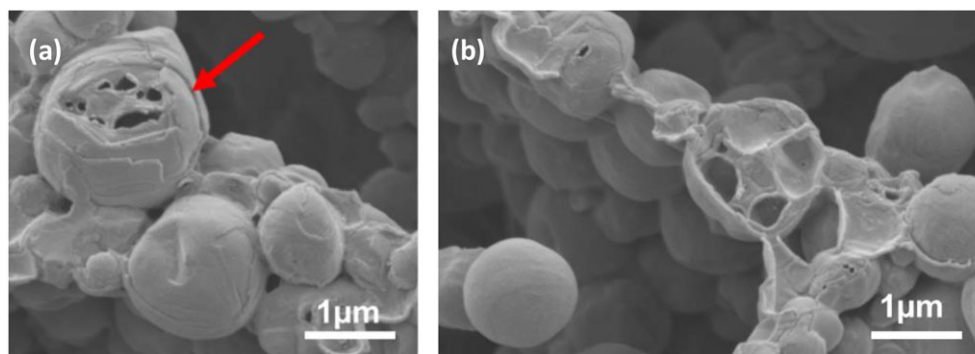

FIGURE 2 (a,b) Cryo-SEM images of the W/O/W$_{sPMF}$ double emulsions after sample preparation (cryogenic freezing and sublimation). SEM: scanning electron microscopy; sPMF: soft palm mid fraction; W/O/W: water-in-oil-in-water
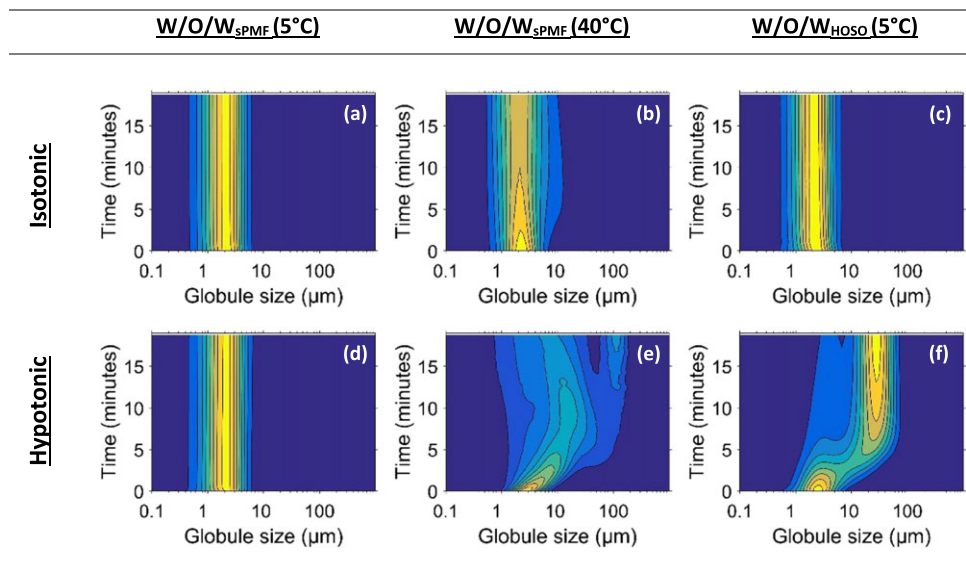
FIGURE 3 Contour plots of the evolution of the volume-weighted diameter distribution of W/O/W double emulsions upon dilution in a hypotonic and isotonic solution. The W/O/W$_{HOSO}$ was measured at 5°C, whereas W/O/W$_{sPMF}$ is measured at 5°C and 40°C. Increasing values in volume percentage (%) are indicated with brighter colors. HOSO: high oleic sunflower oil; sPMF: soft palm mid fraction; W/O/W: water-in-oil-in-water

indeed did not remain stable (Figure 3f). First, the peak mode shifted to larger sizes, and the distribution width increased. Subsequently, the quasimonomodal distribution evolved to a bimodal distribution, of which the second peak grew at the expense of the initial peak. The final $D_{4,3}$ was 27.9 ± 1.2 μm, which is too large to be explained in terms of swelling only. After some initial swelling, insufficient PGPR could have been available to fully cover and stabilize the newly created interfacial area of the internal water droplets. In addition, fat globules will be packed with swollen droplets, separated only by a thin oil film. Coalescence between inner droplets, mutually, and between inner droplets and the fat globule surface will thus probably take place due to film rupture. At the globule level, swelling might identically provoke insufficient coverage by the surfactant (i.e., sodium caseinate) because of the large dilution in the dispersion unit. The emerging second peak is thus likely also related to destabilization due to aggregation and coalescence of the oil globules. The globule size distribution profile of the W/O/W$_{sPMF,40°C}$ double emulsion upon dispersion in a hypotonic solution was also not stable during the experiment (Figure 3e). The peak mode rapidly shifted and broadened, and new peaks emerged. The final distribution profile contains multiple peaks whereof the largest peak is characterized by a mode that exceeds 100 μm, which is rather designated to coagulated globules. The rapid and extensive destabilization of the W/O/W$_{sPMF,40°C}$ double emulsion upon dispersion in a hypotonic solution is believed to have the same origin as the destabilization observed for the W/O/W$_{HOSO,5°C}$ double

emulsion. The difference of the W/O/W$_{sPMF,40°C}$ with the W/O/W$_{HOSO,5°C}$ emulsion is thought to be due to a combination of variations in experimental temperature and yield. First, parallel to Fick's law for passive diffusion of solutes through a barrier, the water flux is proportional to the inverse of the travelling distance, the cross-sectional area (here, interfacial area), and the diffusion coefficient. The latter is on its turn related to the temperature according to the Stokes–Einstein relation. Second, the higher temperature gives rise to a slightly higher osmotic gradient. Third, a higher yield was noted for the W/O/W$_{sPMF}$ emulsion that imposes a thinner oil wall and a larger cross-sectional area. Nevertheless, for both W/O/W$_{HOSO,5°C}$ and W/O/W$_{sPMF,40°C}$, the observed evolution in globule size distribution is believed to be initiated by swelling of the double emulsion caused by water migration from the external to the internal aqueous phase, causing in turn aggregation and coalescence.

For some of the repetitions, a minor shift towards larger globule sizes was observed when the W/O/W$_{sPMF,5°C}$ was dispersed in the hypotonic solution. A very small rise in $D_{4,3}$ from 2.5 ± 0.1 μm to 2.9 ± 0.4 μm was noted when comparing the first and last globule size distribution profiles, respectively. However, these $D_{4,3}$ values are not significantly different (P value = 0.107). This observation complies with Guery et al.[25] who also did not observe an increase in globule dimensions nor a loss of the globule structure upon large deformation stresses due to a positive osmotic gradient in their W/O/W-type emulsion formulated with solid fat. Given the straight contour lines in Figure 3d, the outstanding stability of the

W/O/W$_{sPMF,5°C}$ double emulsion under a large positive osmotic pressure gradient stands in contrast with the pronounced destabilization observed for the liquid oil-based emulsions, that is, W/O/W$_{HOSO,5°C}$ and W/O/W$_{sPMF,40°C}$. The resistance of this solid fat-based W/O/W$_{sPMF,5°C}$ double emulsion to osmotically induced swelling must be primarily due to the contribution of the solid fat crystal network.

3.2.3 | Effect of a negative osmotic gradient

A negative osmotic pressure gradient was hypothesized to induce shrinking of the W/O/W globules provided that a permeable, liquid oil phase was present. Shrinking of the W/O/W$_{sPMF,40°C}$ and W/O/W$_{HOSO,5°C}$ double emulsions due to a hypertonic force appeared to occur in the first minute for both emulsions: in both cases, only the first distribution curve deviates from all other 49 succeeding curves, which are mutually identical and resulted in a final globule diameter (D$_{4,3}$) of 1.8 ± 0.0 μm for both double emulsions (Figure 4b,c). The reduction in globule diameter is appointed to the loss of internal water. Unlike these liquid oil-based emulsions, the globule size distribution profiles of the W/O/W$_{sPMF,5°C}$ double emulsion did not show the same trend upon dilution in a hypertonic solution (Figure 4a). The solid fat seems to be able to prevent emptying of the W/O/W globules. This outcome complies with the observations of Frasch-Melnik et al.,[31] who observed stable Pickering-stabilized double emulsions over a time span of 6 weeks when subjected to a negative osmotic gradient. They ascribed the stability to the smooth crystal shell, which is able to endure the compressive pressure force. In their study, W/O/W emulsions were formulated with a fat blend of sunflower oil and monoglycerides and diglycerides to promote the formation of a smooth fat crystal shell around the internal water droplets. sPMF in our study is expected to form a continuous crystal network throughout the bulk volume of the fat phase. However, the stability observed in our system is also thought to be due to the ability to withstand the compressive pressure force.

3.3 | Water exchange measured with NMR diffusometry

The effect of the Δ-value and oil type on the apparent self-diffusion of the water molecules in the W/O/W-type system was evaluated by means of PFG-NMR diffusion experiments at 5°C. The diffusion attenuation curves clearly seemed to be affected by the oil-type and Δ-value (Figure 5). Concerning the Δ-value, the signal attenuation of the W/O/W$_{sPMF}$ emulsion was much less sensitive to larger diffusion delay times during the signal acquisition than the W/O/W$_{HOSO}$ emulsion. Consequently, the use
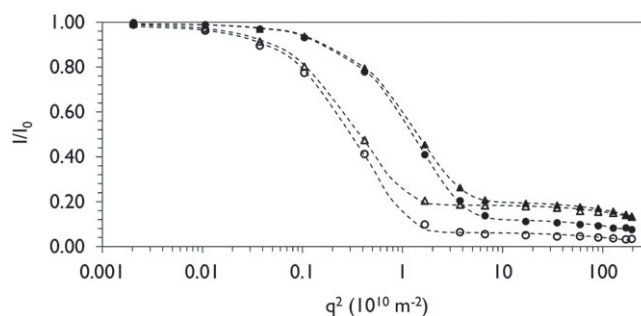

FIGURE 5 Signal attenuation of 30/20/50 (w/w/w) W/O/W emulsions measured by PFG-NMR diffusometry at 5°C for either a diffusion delay time (Δ) of 60 (solid marker) and 220 ms (empty marker). The W/O/W emulsions were formulated either with sPMF (triangle marker) or HOSO (round marker). The dashed lines represent the biexponential fit to the data points
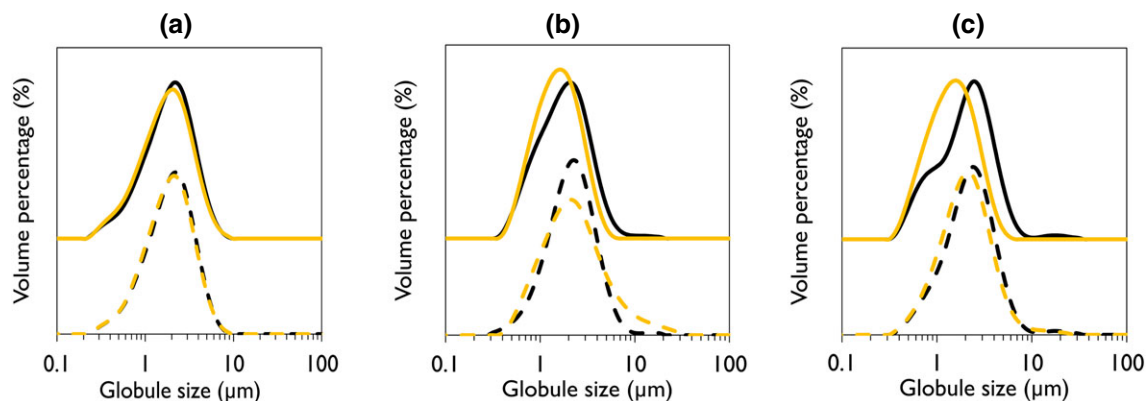

FIGURE 4 First (black) and last (yellow) volume-weighted diameter distribution profiles of the (a) W/O/W$_{sPMF,5°C}$, (b) W/O/W$_{sPMF,40°C}$, and (c) W/O/W$_{HOSO,5°C}$ double emulsions upon dilution in a hypertonic (full line) and isotonic (dashed line) solution. HOSO: high oleic sunflower oil; sPMF: soft palm mid fraction; W/O/W: water-in-oil-in-water

of Equation (2) resulted in a much smaller apparent EV for the W/O/W$_{HOSO}$ emulsion as measured at a Δ-value of 220 ms as compared with a Δ-value of 60 ms (Table 1). This Δ-dependent EV is caused by extradroplet water exchange,[47] which is known to induce a lower apparent EV with increasing Δ-values. Hence, water transport between the internal water droplets and the continuous water phase is assumed to take place in the case of liquid oil-based double emulsions. However, in case of the W/O/W$_{sPMF}$ emulsion, much less water exchange seemed to take place, based on the much smaller decrease in EV with increasing Δ-values, which may be attributed to hampering of water exchange in the W/O/W$_{sPMF}$ globules. The solubility and diffusivity of water molecules in the oil phase take a primary role concerning the permeability of the oil layer. A continuous fat crystal network can complicate molecular diffusion. Pore size, porosity, and pore connectivity characterize the porous fat matrix by a tortuosity factor, which has a considerable impact on the diffusivity of transporting molecules through the porous medium.[48] Evaluation of the water-exchange kinetics by LR-NMR diffusometry provided hereby a fast and nondestructive tool to screen the oil phase permeability without the addition of a marker compound.

TABLE 1 Apparent enclosed water volume (%; with standard deviation) of the W/O/W$_{HOSO}$ and W/O/W$_{sPMF}$ emulsions determined by biexponential fitting of the signal attenuation curve obtained by PFG-NMR diffusometry with a Δ-value of 60 and 220 ms after overnight storage at 5°C

Δ-value (ms)	W/O/W$_{HOSO}$	W/O/W$_{sPMF}$
60	12.4 ± 0.1	20.1 ± 0.1
220	6.5 ± 0.2	18.5 ± 0.2

Note. HOSO: high oleic sunflower oil; PFG-NMR: pulsed field gradient NMR; sPMF: soft palm mid fraction; W/O/W: water-in-oil-in-water.

3.4 | Evaluation of manganese permeation

The migration of manganese ions from the external to the internal water phase in double emulsions can be qualitatively determined by use of ^{1}H-T$_2$-relaxometry.[27] Upon addition of MnCl$_2$ to the external water phase, the internal and external water phase of the W/O/W emulsion can be distinguished thanks to their different T$_2$-relaxation times. At 5°C, the Mn^{2+}-spiked water, that is, the external water phase, relaxes between 10 and 100 ms, whereas the water captured in the internal droplets has relaxation times between 0.1 and 1 s provided that it remains protected from the externally added Mn^{2+} ion. For the sake of completeness, the liquid oil phase also relaxes at T$_2$ times below 100 ms and bulk water typically shows relaxation times around 1 s at 5°C. Consequently, the MnCl$_2$ spiked external water phase becomes indiscernible from the oil phase upon MnCl$_2$ addition to the W/O/W samples. Hence, the smaller peak at larger T$_2$ values, which corresponds to the internal water upon MnCl$_2$ addition, is more relevant to this work. Table 2 shows the modes (W) and integrated peak areas (A) of the T$_2$-distributions of the manganese-spiked W/O/W$_{HOSO}$ and W/O/W$_{sPMF}$ double emulsions during storage at 5°C. The integrated peak area of the slowly relaxing water pool (A$_{SLOW}$) is defined as the water that relaxes at T$_2$ values larger than 100 ms (W$_{SLOW}$). In the presence of Mn^{2+}, this corresponds only to the internal water whereas in the absence of Mn^{2+}, it represents all water present. The fast relaxing water (W$_{FAST}$) is thus referred to as the water that relaxes at T$_2$ values smaller than 100 ms. As mentioned above, this peak also contains the oil signal, whereby oil might interfere with the W$_{FAST}$ value. Hence, A$_{SLOW}$ and W$_{SLOW}$ are the main parameters of interest. The integrated areas in Table 2 are normalized by dividing the signal area with the total integrated area.

TABLE 2 The modes of the T$_2$-distributions of the fast and slowly relaxing water pools (W$_{FAST}$ and W$_{SLOW}$, respectively) and the normalized integrated area of the slowly relaxing water (A$_{SLOW}$) of the manganese-spiked W/O/W$_{HOSO}$ and W/O/W$_{sPMF}$ double emulsions during storage at 5°C

	T$_2$ (ms) of W$_{FAST}$		T$_2$ (ms) of W$_{SLOW}$		A$_{SLOW}$ (%)	
Day	W/O/W$_{HOSO}$	W/O/W$_{sPMF}$	W/O/W$_{HOSO}$	W/O/W$_{sPMF}$	W/O/W$_{HOSO}$	W/O/W$_{sPMF}$
0	33 ± 0	30 ± 0	310 ± 16	567 ± 30	8.2 ± 0.5	16.8 ± 0.1
1	35 ± 2	30 ± 0	283 ± 15	659 ± 0	8.1 ± 0.5	16.8 ± 0.0
4	36 ± 0	30 ± 0	292 ± 27	585 ± 30	7.1 ± 0.6	16.3 ± 0.7
14	37 ± 2	31 ± 2	360 ± 19	397 ± 56	4.0 ± 0.2	14.3 ± 0.3
21	36 ± 0	33 ± 0	291 ± 0	396 ± 40	3.9 ± 0.1	13.0 ± 0.1
35	40 ± 0	33 ± 0	339 ± 17	340 ± 37	2.4 ± 0.1	11.4 ± 0.5

Note. Average values are given with standard deviation based on three measurements. HOSO: high oleic sunflower oil; sPMF: soft palm mid fraction; W/O/W: water-in-oil-in-water.

The T_2-relaxation distributions at day 0 (i.e., obtained 20 min after $MnCl_2$ addition) revealed that the internal, slowly relaxing water (W_{SLOW}) of the W/O/W$_{HOSO}$ emulsion was more affected by the addition of $MnCl_2$ to the external aqueous phase than the W/O/W$_{sPMF}$ emulsion (Figure 6): A larger shift of W_{SLOW} to smaller T_2 values was found for the W/O/W$_{HOSO}$ emulsion. The peak maximum was found at a T_2 value of 310 ± 16 ms for the W/O/W$_{HOSO}$ emulsion whereas at 567 ± 30 ms for the W/O/W$_{sPMF}$ emulsion (Table 2), which indicates a more pronounced Mn^{2+} influx in the former case. Furthermore, the T_2-relaxation distributions were affected by the storage time. Regardless of the oil type, the peak area of the slowly relaxing mode (A_{SLOW}) decreased in time (Table 2). At Day 35, only one third of the enclosed water was affected in case of the W/O/W$_{sPMF}$ emulsion, whereas for the W/O/W$_{HOSO}$ emulsion, more than two third of the enclosed water was affected. This implies that either Mn^{2+} was able to migrate to the internal water droplets with as result that these manganese-affected water droplets contribute to the integrated signal intensity of the fast relaxing water protons instead of the A_{SLOW} signal or that a net water transport takes place from the internal droplets to the continuous phase. The former event would reflect an apparent reduction in W_{SLOW}, whereas the latter, a real reduction of W_{SLOW}. In this respect, the $EV_{\Delta \to 0}$ at Day 0 and day 35 obtained by NMR diffusometry was noted to be 20.8% and 21.3%, respectively, in case of the W/O/W$_{sPMF}$ emulsion and was 14.6% and 13.0%, respectively, for the W/O/W$_{HOSO}$ emulsion. For both emulsions, the decrease in A_{SLOW} during storage could thus not be explained (solely) in terms of internal water loss. This demonstrates that the manganese ions must migrate to the internal water droplets. A part of the internal water droplets contributed as such also to the integrated signal intensity of the fast relaxing water protons instead of A_{SLOW}. Moreover, the

peak maximum of W_{FAST} shifted for both the W/O/W$_{HOSO}$ and W/O/W$_{sPMF}$ emulsions to higher relaxation times upon storage (Table 2). This upward trend might be attributed to lower concentrations of the paramagnetic probe in the continuous water phase due to the manganese migration to the internal aqueous phase. Again, this effect was more pronounced for the liquid oil-containing W/O/W emulsion as compared with the solid fat-containing W/O/W emulsion. The peak maximum of W_{SLOW} showed only for the W/O/W$_{sPMF}$ emulsion a trend to lower T_2 values, whereas no trend could be found for the W/O/W$_{HOSO}$ emulsion. The reduction in T_2 value of the W_{SLOW} is attributed to water droplets, which are affected by very little amounts of Mn^{2+} caused by limited Mn^{2+} influx. This influx was high enough to mark a reduction in T_2 values but was too low to give the water droplets the same low T_2 value as the external Mn^{2+}-spiked aqueous phase. Only after 35 days, the T_2-relaxation time of the internal water of the solid fat-containing W/O/W becomes comparable with the value of the liquid oil-containing W/O/W emulsion, which is again in line with the hypothesis of slower Mn^{2+} migration through the solid fat phase. Overall, it seems that the W/O/W$_{sPMF}$ double emulsion consisted of a water droplet population of which certain droplets were very little affected by manganese permeation (reflected by the T_2 value reduction of W_{SLOW}) whereas other droplets were prone to the influx of Mn^{2+} (reflected by the A_{SLOW} reduction) within the time frame considered. We hypothesize that the droplets that were only little affected by Mn^{2+} influx were protected to a greater extent by the fat crystals and might be located more in the core of the W/O/W globule, whereas the droplets that were more prone to the Mn^{2+} influx were less protected by being located closer to the external interface that reduces the travel distance for Mn^{2+} ions. The Mn^{2+}-ion transport might be credited to PGPR carrier transport[49,50] along
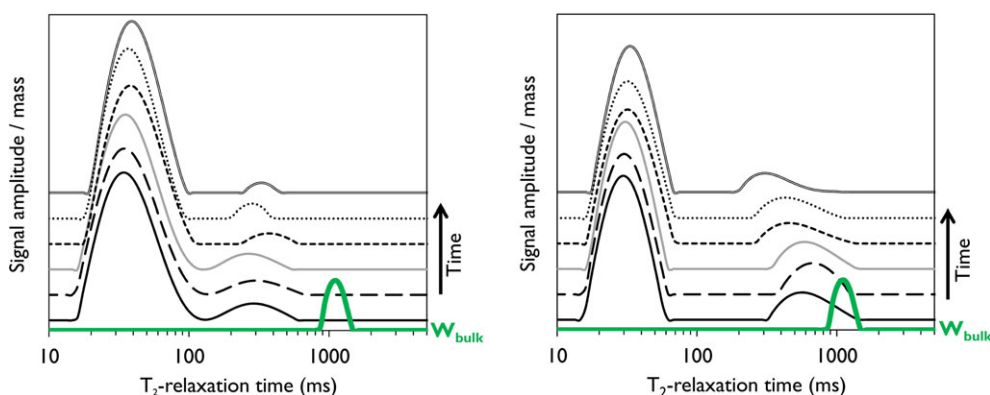

FIGURE 6 T_2-relaxation time distributions of the W/O/W$_{HOSO}$ (left) and W/O/W$_{sPMF}$ (right) double emulsions upon addition of 2.5% (*v/v*) 10-mM $MnCl_2$ during storage at 5°C: Day 0 (20 min), Day 1, Day 4, Day 14, Day 21, and Day 35, and of bulk water (W$_{bulk}$; rescaled). HOSO: high oleic sunflower oil; sPMF: soft palm mid fraction; W/O/W: water-in-oil-in-water

with the diffusion or permeation mechanism given the finite solubility of Mn^{2+} in the oil phase as described for magnesium ions,[10,26,51] chloride ions,[25] and paramagnetic gadolinium complexes.[50] For the sake of completeness, it has to be mentioned that the contribution of $MnCl_2$ to the external osmotic pressure (i.e., 3 kPa at 5°C) is very small (i.e., less than 1%) compared with the initial large osmotic pressures in both the internal and external aqueous phases. Therefore, water transfer due to $MnCl_2$ addition was considered negligible. In addition, no structural changes of the W/O/W globules were observed by light microscopy.

4 | CONCLUSION

In this manuscript, we demonstrated that network crystallization in the oil phase of a W/O/W double emulsion reduced molecular transport through the oil phase. The ability to tune the oil phase permeability by fat crystallization in the oil volume is a very promising tool to control the retention and release of hydrophilic encapsulated compounds with respect to functional food systems. Whereas most other research focused on the leakage of only one encapsulated marker compound during long-term storage,[24–26] we proved the effectiveness of a crystal network as a physical barrier in W/O/W globules by three different types of experiments. Water transport was assessed by low resolution NMR diffusometry under isotonic conditions and by an osmotically induced swelling or shrinking experiment, whereas manganese ion permeation was followed by means of T_2-relaxometry during a 35 days storage experiment. These methods probe exchange at largely different time scales in the order of milliseconds, minutes, and days, respectively.

The stability of the W/O/W$_{sPMF}$ double emulsion towards an osmotic pressure gradient depended on the experimental temperature. The structure of the solid fat-based W/O/W$_{sPMF,5°C}$ globules remained stable under a positive and negative osmotic gradient. In contrast, the liquid oil-based W/O/W$_{HOSO,5°C}$ and W/O/W$_{sPMF,40°C}$ double emulsions experienced extended destabilization upon dilution in a hypotonic and hypertonic medium, which was suggested to be initiated by water uptake and droplet emptying, respectively. The stability of the W/O/W$_{sPMF,5°C}$ system in the observed time frame is suggested to be due to the mechanical strength of the fat crystal network to withstand expansion and compression pressures as previously described.[25] Subsequently, NMR diffusion experiments revealed a reduced water exchange for the W/O/W$_{sPMF}$ emulsion compared with the W/O/W$_{HOSO}$ emulsion. This may be ascribed to the fact that sPMF crystallization induced network crystallization in

the bulk oil volume of the W/O/W$_{sPMF}$ globules, which increased the tortuosity to the migration path of diffusing compounds in the oil phase. Likewise, Mn^{2+} transport was assumed to be slowed down by the increased tortuosity in the sPMF matrix. T_2-relaxometry demonstrated that manganese ion influx was lower when solid fat was present. The slower molecular transport through the oil phase of the solid fat-containing W/O/W$_{sPMF}$ emulsion is in line with previously described network crystallized W/O/W systems.[26]

CONFLICT OF INTEREST

None.

ORCID

Veronique Nelis https://orcid.org/0000-0002-9909-4582
Lien Vermeir https://orcid.org/0000-0002-9768-8010

REFERENCES

[1] G. Muschiolik, E. Dickinson, *Compr. Rev. Food Sci. Food Saf.* **2017**, *16*, 532.

[2] H. Lamba, K. Sathish, L. Sabikhi, *Food Bioprocess Technol.* **2015**, *8*, 709.

[3] D. J. McClements, *Food Emulsions: Principles, Practices, and Techniques*, CRC Press, Boca Raton **2015**.

[4] N. Garti, *Colloids Surfaces A Physicochem. Eng. Asp.* **1997**, *123–124*, 233.

[5] E. Dickinson, *Food Biophys.* **2011**, *6*, 1.

[6] H. L. Rosano, F. G. Gandolfo, J. P. Hidrot, *Colloids Surfaces A Physicochem. Eng. Asp.* **1998**, *138*, 109.

[7] L. Wen, K. D. Papadopoulos, *Colloids Surfaces A Physicochem. Eng. Asp.* **2000**, *174*, 159.

[8] A. Benichou, A. Aserin, N. Garti, *Adv. Colloid Interface Sci.* **2004**, *108–109*, 29.

[9] G. Muschiolik, *Curr. Opin. Colloid Interface Sci.* **2007**, *12*, 213.

[10] S. Herzi, W. Essafi, S. Bellagha, F. Leal-Calderon, *Langmuir* **2012**, *28*, 17597.

[11] J. Bahtz, D. Z. Gunes, E. Hughes, L. Pokorny, F. Riesch, A. Syrbe, P. Fischer, E. J. Windhab, *Langmuir* **2015**, *31*, 5265.

[12] J. Bahtz, D. Z. Gunes, A. Syrbe, N. Mosca, P. Fischer, E. J. Windhab, *Langmuir* **2016**, *32*, 5787.

[13] M. Bonnet, M. Cansell, F. Placin, J. Monteil, M. Anton, F. Leal-Calderon, *Colloids Surfaces B Biointerfaces* **2010**, *78*, 44.

[14] J. Yan, R. Pal, *J. Memb. Sci.* **2001**, *190*, 79.

[15] P. Colinart, S. Delepine, G. Trouve, H. Renon, *J. Memb. Sci.* **1984**, *20*, 167.

[16] Y. Sela, S. Magdassi, N. Garti, *J. Controlled Release* **1995**, *33*, 1.

[17] R. Mezzenga, B. M. Folmer, E. Hughes, *Langmuir* **2004**, *20*, 3574.

[18] L. Wen, K. D. Papadopoulos, *Langmuir* **2000**, *16*, 7612.

[19] L. Wen, K. D. Papadopoulos, *J. Colloid Interface Sci.* **2001**, *235*, 398.

[20] M. Balcaen, L. Vermeir, A. Declerck, P. Van der Meeren, *Food Hydrocolloids* **2016**, *58*, 356.

[21] A. K. L. Oppermann, M. Renssen, A. Schuch, M. Stieger, E. Scholten, *Food Hydrocolloids* **2015**, *48*, 17.

[22] M. Bonnet, M. Cansell, A. Berkaoui, M. H. Ropers, M. Anton, F. Leal-Calderon, *Food Hydrocolloids* **2009**, *23*, 92.

[23] S. Kiokias, A. A. Reszka, A. Bot, *Int. Dairy J.* **2004**, *14*, 287.

[24] J. Weiss, I. Scherze, G. Muschiolik, *Food Hydrocolloids* **2005**, *19*, 605.

[25] J. Guery, J. Baudry, D. A. Weitz, P. M. Chaikin, J. Bibette, *Phys. Rev. E - Stat. Nonlinear, Soft Matter Phys.* **2009**, *79*, 1.

[26] S. Herzi, W. Essafi, *J. Colloid Interface Sci.* **2018**, *509*, 178.

[27] L. Vermeir, M. Balcaen, P. Sabatino, K. Dewettinck, P. Van der Meeren, *Colloids Surfaces A Physicochem. Eng. Asp.* **2014**, *456*, 129.

[28] L. Vermeir, P. Sabatino, M. Balcaen, A. Declerck, K. Dewettinck, J. C. Martins, G. Guthausen, P. Van der Meeren, *J. Colloid Interface Sci.* **2016**, *475*, 57.

[29] N. Garti, A. Aserin, I. Tiunova, H. Binyamin, *JAOCS, J. Am. Oil Chem. Soc.* **1999**, *76*, 383.

[30] S. Frasch-Melnik, I. T. Norton, F. Spyropoulos, *J. Food Eng.* **2010**, *98*, 437.

[31] S. Frasch-Melnik, F. Spyropoulos, I. T. Norton, *J. Colloid Interface Sci.* **2010**, *350*, 178.

[32] F. Spyropoulos, S. Frasch-Melnik, I. T. Norton, *Procedia Food Sci.* **2011**, *1*, 1700.

[33] M. Nadin, D. Rousseau, S. Ghosh, *LWT - Food Sci. Technol.* **2014**, *56*, 248.

[34] V. Jenning, M. Schäfer-Korting, S. Gohla, *J. Controlled Release* **2000**, *66*, 115.

[35] R. Müller, *Eur. J. Pharm. Biopharm.* **2000**, *50*, 161.

[36] J. Weiss, E. A. Decker, D. J. McClements, K. Kristbergsson, T. Helgason, T. Awad, *Food Biophys.* **2008**, *3*, 146.

[37] R. H. Müller, M. Radtke, S. A. Wissing, *Adv. Drug Delivery Rev.* **2002**, *54*, S131.

[38] A. Declerck, V. Nelis, T. Rimaux, K. Dewettinck, P. Van der Meeren, *Eur. J. Lipid Sci. Technol.* **2018**, *120*, 1.

[39] E. O. Stejskal, J. E. Tanner, *J. Chem. Phys.* **1965**, *42*, 288.

[40] A. Declerck, *Characterisation and Quantification of Fat Crystallisation in Bulk Fat and Double Emulsions*, PhD Thesis, Ghent University, Belgium **2019**.

[41] E. Trezza, A. M. Haiduc, G. J. W. Goudappel, J. P. M. van Duynhoven, *Magn. Reson. Chem.* **2006**, *44*, 1023.

[42] W. S. Provencher, *Comput. Phys. Commun.* **1982**, *27*, 213.

[43] P. Sabatino, P. Saveyn, J. C. Martins, P. Van Der Meeren, *Langmuir* **2011**, *27*, 4532.

[44] V. Gibon, J. V. Ayala, P. Dijckmans, J. Maes, W. De Greyt, *OCL - Oilseeds fats, Crop. Lipids* **2009**, *16*, 193.

[45] A. G. Marangoni, N. Acevedo, F. Maleky, E. Co, F. Peyronel, G. Mazzanti, B. Quinn, D. Pink, *Soft Matter* **2012**, *8*, 1275.

[46] V. Nelis, A. Declerck, L. De Neve, K. Moens, K. Dewettinck, P. Van der Meeren, *Colloids Surfaces A Physicochem. Eng. Asp.* **2019**, *566*, 196. https://doi.org/10.1016/J.COLSURFA.2019.01.019

[47] L. Vermeir, M. Balcaen, A. Declerck, P. Van der Meeren, *Proc. XIII Int. Conf. Appl. Magn. Reson. Food Sci.* **2016**, *61*.

[48] F. Maleky, A. Marangoni, *Soft Matter* **2011**, *7*, 6012.

[49] S. J. Choi, E. A. Decker, L. Henson, L. M. Popplewell, D. J. McClements, *Food Chem.* **2010**, *122*, 111.

[50] R. Bernewitz, F. Dalitz, K. Köhler, H. P. Schuchmann, G. Guthausen, *Microporous Mesoporous Mater.* **2013**, *178*, 69.

[51] S. Herzi, W. Essafi, S. Bellagha, F. Leal-Calderon, *Colloids Surfaces a Physicochem. Eng. Asp.* **2014**, *441*, 489.

SUPPORTING INFORMATION

Additional supporting information may be found online in the Supporting Information section at the end of the article.